

1 **Parameterization of atmospheric long-wave emissivity in a mountainous site for all sky** 2 **conditions**

3 Herrero, J.^{1*} and Polo, M.J.²

4 ¹ Fluvial Dynamics and Hydrology Research Group, Instituto Interuniversitario del Sistema Tierra en Andalucía,
5 University of Granada, Spain.

6 ² Fluvial Dynamics and Hydrology Research Group, Instituto Interuniversitario del Sistema Tierra en Andalucía,
7 Campus de Excelencia Internacional Agroalimentario ceiA3, University of Cordoba, Spain

8 *Corresponding author. Edf. CEAMA. Av. del Mediterráneo s/n. 18006. Granada. Spain. email: herrero@ugr.es.
9 Tef: 0034 958249743. Fax: 0034 958132479

11 **Abstract**

12 Long-wave radiation is an important component of the energy balance of the Earth's
13 surface. The downward component, emitted by the clouds and aerosols in the atmosphere, is
14 rarely measured, and is still not well understood. In mountainous areas, the models existing for
15 its estimation through the emissivity of the atmosphere do not give good results, and worse still
16 in the presence of clouds. In order to estimate this emissivity for any atmospheric state and in a
17 mountainous site, we related it to the screen-level values of temperature, relative humidity and
18 solar radiation. This permitted the obtaining of: (1) a new set of parametric equations and (2)
19 the modification of Brutsaert's equation for cloudy skies through the calibration of C factor to
20 0.34 and the parameterization of the cloud index N . Both fitted to the surface high-resolution
21 data measured at a weather station at a height of 2500 m a.s.l. in Sierra Nevada, Spain. This
22 study analyzes separately three significant atmospheric states related to cloud cover, which
23 were also deduced from the screen-level meteorological data. The validation of the expressions
24 in two alternative sites shows that the superior accuracy in the new 3-state parametric equation
25 is restricted to local use. On the other hand, parameterization of cloud influence in Brutsaert's
26 equation through the use of screen-level measurements of relative humidity and solar radiation
27 can provide a simple expression to calculate instantaneous atmospheric emissivity of a broader
28 applicability.

30 **1 Introduction**

31 Long-wave radiation has an outstanding role in most of the environmental processes
32 that take place near the Earth's surface (e.g., Philipona, 2004). Radiation exchanges at
33 wavelengths longer than 4 μm between the Earth and the atmosphere above are due to the
34 thermal emissivity of the surface and atmospheric objects, typically clouds, water vapour and
35 carbon dioxide. This component of the radiation balance is responsible for the cooling of the

36 Earth's surface, as it closely equals the shortwave radiation absorbed from the sun. The
37 modelling of the energy balance, and, hence, of the long-wave radiation balance at the surface,
38 is necessary for many different meteorological and hydrological problems, e.g., forecast of
39 frost and fog, estimation of heat budget from the sea (Dera, 1992), simulation of evaporation
40 from soil and canopy, or simulation of the ice and snow cover melt (Armstrong and Brun,
41 2008).

42 Even though long-wave radiation instrumentation (pyrgeometer) is nowadays usually
43 deployed at weather stations specifically designed for scientific purposes (e.g., Sicart et al.,
44 2006), it is not so common in the most habitual automated weather stations. Hence, all energy
45 balance models estimate long-wave components independently through different physical
46 relations and parameterizations. Downward long-wave radiation is difficult to calculate with
47 analytical methods, as they require detailed measurements of the atmospheric profiles of
48 temperature, humidity, pressure, and the radiative properties of atmospheric constituents
49 (Alados et al., 1986; Lhomme et al., 2007). To overcome this problem, atmospheric emissivity
50 and temperature profile are usually parameterized from screen level values of meteorological
51 variables. The use of near surface level data is justified since most incoming long-wave
52 radiation comes from the lowest layers of the atmosphere (Ohmura, 2001).

53 It is relatively easy to create parameterizations to estimate emissivity under clear sky
54 conditions. Several studies have compared the performance of different parameterizations over
55 long-wave records (e.g., Sugitia and Brutsaert, 1993; Gabathuler et al., 2001) and for all cloudy
56 sky conditions (Pluss and Omhura, 1996; Crawford and Duchon, 1999; Pirazzini et al., 2000;
57 Kjaersgaard et al., 20007; Sedlar and Hock, 2009, Staiger and Matzarakis, 2010). But only a
58 few of them were carried out on highland sites (Iziomon et al., 2003; Lhomme et al., 2007;
59 Flerchinger et al., 2009). Besides, the effect of clouds and stratification on atmospheric
60 emissivity is highly dependent on regional factors, which may lead to the need for local
61 expressions (e.g., Alados et al., 1986; Barbaro, et al., 2010).

62 But mountainous catchments are very sensitive areas as they are greatly exposed to
63 meteorological conditions. Here, the surface energy balance has the greatest influence on
64 environmental processes, especially if snow is present. As existing measurements are scarce
65 (e.g., Iziomon et al., 2003; Sicart et al., 2006), a correct parameterization of downward long-
66 wave irradiance under all sky conditions is essential for these areas. Herrero et al. (2009)
67 modelled the energy balance of the snowpack in Sierra Nevada Mountains (Spain), by the
68 Mediterranean sea. Different parameterizations for atmospheric long-wave emissivity (Brunt,
69 1932; König-Langlo and Augstein, 1994; Prata, 1996) were tested for clear sky periods, and
70 although the best model performance was obtained using Brutsaert (1975) (same as Kimball et

71 al., 1982; Kustas et al., 1994; Iziomon et al., 2003), the extension to cloudy conditions (e.g.
72 with Crawford and Duchon, (1999)) turned into a global underestimation of incoming long-
73 wave radiation. This underestimation prevented the model from reproducing the different
74 winter snow melting cycles typical of this Mediterranean low-latitude area. This problem was
75 overcome through the use of a simple parameterization for atmospheric emissivity based on 2-
76 yr screen level values of solar radiation, temperature and relative humidity that greatly
77 improved the simulation of the snow cover evolution (Herrero et al., 2009).

78 In this work, a deeper analysis of long-wave incoming radiation through measurements
79 and its relation to other meteorological data in a high mountain site is presented. From this
80 analysis, a local parameterization for atmospheric emissivity under all sky conditions, based on
81 5-min surface measurements of relative humidity, temperature, and solar radiation is proposed
82 and validated against direct local measurements. For this purpose, two different approaches
83 were performed: (1) a new empirical expression for Sierra Nevada from 5 yr of surface
84 meteorological data furthering the results in Herrero et al. (2009); (2) a modification of
85 Brutsaert's equation (Brutsaert, 1982) by means of the parameterization of its cloudiness-
86 related index, N .

87

88 **2 Site description and instrumentation**

89 The study site is the Southern slope of Sierra Nevada Mountain (Fig. 1), located 35 km
90 north from the Mediterranean Sea in Southeastern Spain (37.5° N). This mountain range raises
91 3500 m a.s.l. and runs parallel to the sea for approximately 60 km. It is characterized by high
92 altitudinal gradients and a heterogeneity produced by a high mountain climate influenced by
93 the surrounding Mediterranean climate. The presence and influence of winter snow becomes
94 important at above 2000 m a.s.l. The snowmelt season generally extends from April to June,
95 even though the mild winter periods characteristic of the Mediterranean climate can melt most
96 of the snow before the end of the snow season (especially during January and February).
97 Typically, several consecutive accumulation/melting cycles take place during one year.
98 Sublimation from the snow can also be very important, up to 40% of year snow precipitation, if
99 the appropriate meteorological conditions prevail (Herrero et al., 2009). Sierra Nevada houses
100 a Spanish National Park and one of the International Global Change Observatories in Mountain
101 Areas because of its particular conditions and delicate environment.

102 An automatic weather station was operated in Refugio Poqueira (RP Station), at 2500 m
103 a.s.l. (Herrero et al., 2011). Measurements of incoming shortwave and long-wave radiation
104 (Kipp&Zonen SP-Lite pyranometer and CGR3 pyrgeometer), and 2-m air temperature and
105 relative humidity (Vaisala HMP45), among others, have been conducted continuously since

106 November 2005. The CGR3 pyrgeometer has a spectral range comprised between 4.5 and 44
107 μm and an accuracy of 5 Wm^{-2} . A Campbell CR-510 datalogger recorded 5-min averages of 5s
108 sampling rate observations. Additionally, for this study we have used the data recorded by two
109 new weather stations installed in the proximity of RP Station in 2009 that were equipped with
110 downward long-wave sensors: (1) EN2 Station, belonging to the Department of Agriculture,
111 Fishing and Environment of the Regional Government of Andalusia, is located at only 4 km
112 East from RP Station and at 2325 m a.s.l., within the same Southern slope of Sierra Nevada.
113 Radiation is measured by a NR01 Hukseflux 4-component net radiometer, while temperature
114 and relative humidity are measured by a Vaisala HMP45. Data are recorded at 10-min intervals.
115 (2) Contraviesa Station (C Station) is located 25 km South from RP Station at 1332 m a.s.l., on
116 the ridge of Contraviesa mountain range, which is a lower range parallel to Sierra Nevada. It
117 has the same configuration as RP Station, except from the radiation sensors, which, in this case,
118 are an IR02 pyrgeometer and a LP02 pyranometer, both from Hukseflux.

119

120 **3 Data analysis**

121 **3.1 Long-wave data**

122 After the Stefan-Boltzmann Law for the radiation emission of any body at a
123 temperature T (K), downward long-wave radiation L^\downarrow (Wm^{-2}) coming from the near-surface
124 layer of the atmosphere may be written as:

125

$$126 \quad L^\downarrow = \varepsilon_a \sigma T_a^4 \quad (1)$$

127

128 where ε_a is the apparent emissivity of the sky (Unsworth and Monteith, 1975), σ ($\text{Wm}^{-2}\text{K}^{-4}$) is
129 the Stefan-Boltzmann constant, and T_a (K) is the air temperature near the surface (typically 2
130 m).

131 The downward long-wave radiation measured for 5 consecutive years at RP Station,
132 converted to ε_a according to Eq. (1), is shown on Fig. 2a and summarized in the probability
133 density function (pdf) in Fig. 3. The lower values of ε_a belong to clear sky situations, and in the
134 pdf they smoothly fit a Gaussian with a mean value of 0.68 and a standard deviation of 0.0565.
135 During very clear days, with a low temperature and relative humidity, it exhibits values ranging
136 from 0.5 to 0.6. In the pdf, 0.77 sets the limit between clear sky and partly covered situations;
137 higher values of ε_a denote the presence of clouds in the atmosphere. A seasonal pattern is easily
138 observed in Fig. 2.a, where the lowest emissivity values from clear skies are reached during
139 winter. This emphasizes the importance of long-wave balance for cooling the soil and snow
140 under high mountain clear skies. These measurements are similar to those found by Frigerio

141 (2004) in Argentina, at 2300 m a.s.l., with night values of atmospheric emissivity of under 0.7
142 with clear skies. Figure 2b represents daily variation of ε_a , that is, the difference between
143 maximum and minimum daily values. It exhibits a marked seasonality, where wider daily
144 variations of ε_a in winter are in accordance with wider variations in temperature and relative
145 humidity. Minimum instantaneous values of ε_a during winter can be as low as 0.4, while in
146 summer they rarely drop to under 0.6.

147 These measured values are lower than those estimated from the usual empirical
148 expressions, which casts a doubt over the latter for their general use in the highland under any
149 atmospheric state. Thus, the expression by König-Langlo and Augstein (1994), used by Jordan
150 (1999) in the SNTHERM model, gives a minimum value for emissivity of 0.765, much higher
151 than the real values measured in this site. Prata (1996) also overestimates the lower values
152 found under clear skies. Only Brutsaert (1975) gives more realistic values of ε_a for clear skies,
153 and is capable of reproducing values of below 0.60 during cold days with a clear sky and low
154 relative humidity.

155 **3.2 Parameterizations from screen-level data**

156 From the previous analysis of the data recorded by RP Station, it was found that relative
157 humidity, W_a , exhibited more compact relations with ε_a and T_a than the water vapour pressure,
158 e_a . So, despite e_a being the variable commonly used in the calculation of ε_a for clear skies, W_a
159 was chosen for the parameterizations because it seems to represent the variation in ε_a better due
160 to the presence of water in the atmosphere at high altitudes. Figure 4a shows the relationship
161 between the measured values of ε_a , T_a , and W_a for all sky conditions. That relationship is
162 especially strong for clear and completely covered skies, as shown by the low magnitudes of
163 the standard deviation (std) in Fig. 4b for the values of ε_a under 0.7 and over 0.9, respectively.
164 Partly covered skies appear as a transition zone between these two boundary situations. There
165 are some differences in these relationships between daytime and night-time values, but they
166 were not found to be significant for these particular data.

167 In order to evaluate the relationship existing between ε_a and cloudiness, the Clearness
168 Index CI has been used, as in Sugita and Brutsaert (1993), and equivalent to ratio s in Crawford
169 and Duchon (1999). CI is the ratio between the theoretical shortwave irradiance at the top of
170 the atmosphere (extraterrestrial radiation) and the surface-measured solar radiation. By means
171 of the CI, calculated with the topographical model described in Aguilar et al. (2010), it is
172 possible to find out the degree of opacity of the atmosphere due to the concentration of
173 aerosols and clouds during the hours with sunshine. Figure 5 shows how the states of clear sky
174 (region A) and sky completely overcast (region B) are very well represented in the relation W_a -
175 CI- ε_a . The transition area between both regions concentrates the dispersion of the values (a

176 high std). The region of the completely covered skies has a very high emissivity, of above 0.95.
 177 This means that not only are there clouds but also that they are close to the surface, which is
 178 common in mountainous areas and the reason why the relative humidity of air is highly
 179 correlated with cloudiness.

180 Thus, a clear sky region (A in Fig. 5a) and a completely overcast region (B in Fig. 5b)
 181 were identified from the analyses of the mean values (Fig. 5a) and their std (Fig 5b). These
 182 regions were delimited by the following expressions as a function of W_a and CI:

183

184 Region A: $CI > 0.25 W_a^2 + 0.025 W_a + 0.65$ (2a)

185 $CI < -0.25 W_a^2 - 0.625 W_a + 1.49$ (2b)

186 Region B: $CI < 2.667 W_a - 1.867$ (3)

187

188 where W_a is expressed as a fraction of one. This partition was made on the basis of the relation
 189 between CI, W_a and emissivity as shown in Fig. (5). Region A for clear skies defines the area
 190 in a CI- W_a axes, where the mean value for the emissivity is lower than 0.7. Conversely, region
 191 B for completely covered skies delimits the area where emissivity is greater than 0.9. It must
 192 be emphasized that these two regions include most of the atmospheric states found, since 59%
 193 of all the daily states are clear skies and 14% are completely covered skies. The intermediate
 194 states correspond to partly cloudy skies or anomalies in the two previous regions, so that it is a
 195 zone with a great dispersion in the values of ϵ_a .

196 For “clear sky” conditions, the following expression for atmospheric emissivity ϵ_a^{cs} was
 197 derived from a polynomial fit of the available screen-level measurements at daytime, where the
 198 non-significant terms have been neglected:

199

200 $\epsilon_a^{cs} = -1.17 + 0.16 W_a + 0.0062 T_a$ (4)

201

202 where W_a is expressed again as a fraction of one and T_a in K. In the case of the “completely
 203 covered skies”, the emissivity ϵ_a^{ccs} does not show any relation to T_a but it does to CI. Therefore,
 204 the following parametric function was fitted, the variables being expressed as before:

205

206 $\epsilon_a^{ccs} = 1 - 1.38 CI + 1.33 W_a CI$ (5)

207

208 For “partly covered skies”, the best fitted expression of the emissivity ϵ_a^{pcs} obtained
 209 was:

210

211 $\varepsilon_a^{\text{PCS}} = 0.81 - 0.26 \text{ CI}^2 + 0.25 W_a^3$ (6)

212

213 Alternatively, a correction of the Brutsaert equation extended to cloudy conditions (Eq.
 214 87), which had proven to be the expression for emissivity that performed best at this site
 215 (Herrero et al., 2009), has been developed. Brutsaert (1982) extended $\varepsilon_a^{\text{CS}}$ for all sky conditions
 216 by means of a factor F :

217

218 $\varepsilon_a = \varepsilon_a^{\text{CS}} F = 1.72 (e_a/T_a)^{1/7} (1 + C N^2)$ (7)

219

220 where e_a is the vapour pressure near the surface in kPa, and $F (\geq 1)$ is the increase in the sky
 221 emissivity due to the presence of clouds. This factor is split in N , a cloud index varying
 222 between 0 for clear skies and 1 for totally overcast skies, and C , an empirical factor dependent
 223 on the cloud types. Since there are no direct measurements of cloudiness, N has been
 224 parameterized using the actual screen-level values of W_a and CI in Eq. (7). This was achieved
 225 by comparing measured and simulated ε_a . C was also calibrated in the process, with a value of
 226 0.34 being obtained.

227

228 $N = 1 - 0.45 \text{ CI} - 3.5 W_a \text{ CI} + 4 W_a^2 \text{ CI}$ (8)

229

230 The value of N obtained from Eq. (8) is never allowed to be lower than 0 or greater than
 231 1.

232 Equations (2) to (8) have been obtained from a calibration dataset composed of all the
 233 5-min data from November, 2004, to December, 2010, including daytime records for any
 234 cloudiness degree.

235 Crawford and Duchon (1999) developed a similar model to the modified Brutsaert
 236 equation proposed for ε_a in Eq. 7 and 8. Also based on Brutsaert (1975), the modelling of the
 237 cloudiness relies upon screen-level measurements of temperature, humidity, solar radiation,
 238 and, in addition, atmospheric pressure. Their model includes two modifications to the original
 239 by Brutsaert (1975): (1) extension to cloudy conditions through a simple linear relation
 240 between ε_a and the ratio of the measured solar irradiance to the clear-sky irradiance, s , in fact
 241 equivalent to the propagation of CI across the atmosphere; and (2) the substitution of the
 242 leading coefficient, lc , (1.72 in Eq. 7) by:

243

244 $lc = (1.22 + 0.06 \sin[(\text{month}+2) \text{ pi}/6]) 10^{1/7}$ (9)

245

246 where month is the numerical month starting in January (=1). This expression results in a
247 leading factor ranging from 1.78 in January to 1.61 in July. Notice that lc is dimensional so the
248 value of 1.72 in Eq. 7 is defined for e_a in kPa and T in K, this being 1.24 if e_a is in hPa and T in
249 K. This model, CD99, was used for comparison with the two approaches presented so far: the
250 3-state parametric expressions, 3-sParam, and the modified Brutsaert equation, modB82.
251 Besides, variable leading coefficient was tested in an alternative version of modB82, modB82-
252 var, to assess its validity in the meteorological data from Sierra Nevada.

253 These four models were tested against the calibration dataset in RP Station and against
254 three validation datasets: (1) 2011 measurements in RP Station, which approximately represent
255 15% of the whole 5-yr dataset, (2) whole record in C Station (august 2009 – April 2012) and
256 (3) whole record in EN2 Station (October 2009 – March 2012). The goodness of agreement of
257 each model was valued by the common statistics Mean Absolute Error MAE and Root of the
258 Mean Square Error RMSE.

259

260 **4 Results and discussion**

261 Figure 6 shows the comparison between daytime ϵ_a measurements and values estimated
262 by the different models for the calibration period at RP Station. Figure 7 shows the same
263 comparison but for the validation at C Station, the lower study site. The complete results from
264 the statistical analysis of all four models for the calibration and the three validation datasets are
265 shown in Table 1. There, the results for the complete daytime data for each case along with the
266 separation for each of the three atmospheric states (clear, totally covered and partly cloudy
267 skies) are presented.

268 The results from the calibration and validation tests at RP Station agree, so calibration is
269 confirmed for this site. The performance of the 3-sParam model stands out over the rest of
270 models, especially for clear and completely covered skies. Partly cloudy skies are also best
271 represented by 3-sParam, even though the differences in this state are lower. The graphical
272 representation of these transition states in Figs. 6 and 7 shows a greater scattering, while
273 measurements and predictions for clear and overcast states clearly fit more tightly. Brutsaert's
274 equation improves when the variable leading coefficient is used (modB82-var), especially for
275 clear skies. CD99 exhibits an overall good performance, very similar to modB82 and modB82-
276 var models, even though it fails to reproduce higher values of emissivity with completely
277 covered skies. In this atmospheric state, measurements of ϵ_a clearly meet at 1, while CD99
278 never reaches that value.

279 The results of the validation at the lower site of C Station show an outstanding loss of
280 performance of the 3-sParam model, particularly for the lower values of emissivity for clear

281 skies, which are vastly underestimated by this model. The transition state is drawn with much
282 more scattering for this model (Fig. 7c). For this dataset, the variable leading coefficient in
283 modBrut82-var and CD99 is much less effective than the constant coefficient, as opposed to
284 what happened at RP Station. CD99 is also still penalized by its incorrect simulation of higher
285 emissivities, whose measurements are very close to the unity for this site too. modB82 has
286 improved substantially for every atmospheric state and exhibits an outstanding performance
287 (without calibration). ε_a measurements are steadier in this lower site compared to what
288 happened at very high altitudes in RP Station.

289 Finally, the validation at EN2 Station, located at a very high altitude, displays a very
290 similar behaviour and statistics for models 3-sParam and modB82 to that found at RP Station,
291 even though measurements are even more unsteady here than in RP site. However, models
292 modB82-var and CD99 clearly get worse for all atmospheric states. The variable leading
293 coefficient makes both models underestimate emissivity for clear skies, while covered skies
294 with emissivities very close to 1 again are not captured by CD99. 3-stateParam is still the most
295 efficient model, followed by modB82.

296 The classification of the data set in 3 atmospheric states, clear, completely covered, and
297 partly cloudy skies, allows a better adjustment and analysis of the performance of the models.
298 The highest error is concentrated in the intermediate atmospheric states, those with partial
299 cloud cover, where the surface measurements are not capable of representing by themselves the
300 complex state of the atmosphere and the presence of clouds and aerosols in it.

301 From Fig. 6, it can be seen that the lowest values for measured ε_a at RP Station, those
302 between 0.4 and 0.5, are grouped in a scattered cloud of points with an estimated value
303 between 0.6 and 0.7. They are overestimated by all the models. In fact, these measurements are
304 taken under similar atmospheric states, corresponding to sunny winter days with low wind
305 speeds ($< 1\text{ m s}^{-1}$), and this overestimation may be caused by the overheating of the
306 pyrgeometer dome by solar radiation under insufficient ventilation. This effect has already
307 been reported (e.g. Weis, 1981), but it is normally not accounted for as the induced errors are
308 low (Lhomme et al., 2007). However, in this work the errors in measured long-wave radiation
309 may be important for these specific meteorological conditions, with an absolute overestimation
310 in measured ε_a up to 0.2.

311 A C coefficient in the extended Brutsaert equation (Eq. 7) of below 0.34 prevents the
312 high values of ε_a , which are measured in very cloudy states, from being reached by models
313 modB82 and modB82-var. This is a much higher value than the 0.22 originally proposed by
314 Brutsaert (1982). This reflects the fact that, in mountainous areas, the interaction of the clouds

315 with the surface of the terrain and, therefore, their effect on ε_a is much more intense than in
316 valley areas.

317 Clear sky data are well predicted in this mountainous site using the original coefficient
318 of 1.72 in Eq. (7) suggested by Brutsaert (1975). The seasonally variable leading coefficient
319 suggested by Crawford and Duchon (1999) (Eq. 9) causes the Brutsaert equation to
320 underestimate emissivity more than its original formulation in two of the three tested sites,
321 which is the same result found by Kjaersgaard et al. (2007). Consequently, there was no need
322 to correct this coefficient, as was already pointed out by Flerchinger et al (2009).

323

324 **5 Conclusions**

325 The high resolution long-wave measurements recorded in a weather station at an
326 altitude of 2500 m in a Mediterranean climate are not correctly estimated by most of the
327 existing models and frequently used parameterizations. These measurements show a very low
328 atmospheric emissivity for long-wave radiation values with clear skies (up to 0.5) and a great
329 facility for reaching the theoretical maximum value of 1 with cloudy skies. Despite the good
330 behaviour of Brutsaert (1975) for clear skies, the cloudiness effect considered in Brutsaert
331 (1982) cannot be effectively added because of the lack of any cloud index N measurements.
332 The relationships between the screen-level values of temperature, relative humidity, and solar
333 radiation by means of the clearness index with the emissivity under clear and cloudy skies,
334 allows one to define two parametric approaches with good results and a different applicability
335 for estimations of the instantaneous values of the atmospheric emissivity: (1) a complete
336 parametric expression, split into three atmospheric states parametrically regionalized (clear,
337 completely covered and partly covered skies), with an outstanding performance at a very local
338 scale even with the unsteady measurements at high altitude mountainous sites; and (2) a
339 modification of Brutsaert (1982) by means of a parameterization of N from the screen level
340 measurements of humidity and solar radiation and a calibration of C index, set to 0.34. This
341 model has proven to have an overall good performance for all atmospheric states and, more
342 important, a broader scope of applicability at different sites without further calibration.

343 The use of a seasonally variable leading coefficient for clear sky emissivity in Brutsaert
344 (1972), as proposed by Crawford and Duchon (1999), was rejected because it underestimates
345 emissivity for clear skies.

346 As a result, it is now possible to obtain atmospheric emissivity series in stations without
347 any long-wave direct measurements, with a direct applicability in the surroundings of Sierra
348 Nevada. Complete parametric expressions should have, in general, a very local scope of
349 applicability, as the validity of these fits is linked to their ability to characterize the state of the

350 atmosphere, with regard to the presence of clouds, only with surface measurements of
351 temperature, humidity, and solar radiation.

352

353 *Acknowledgements.* This work has been carried out within the Guadalfeo Project, funded by
354 the Department of the Environment of the Regional Government of Andalusia, and partially
355 funded by the Spanish Ministry of Science and Innovation (Research Project CGL2011-25632,
356 “Snow dynamics in Mediterranean regions and its modelling at different scales. Implications
357 for water resource management”). Meteorological data at EN2 Station is funded by the Sierra
358 Nevada Global Change Observatory, Department of Agriculture, Fishing and Environment of
359 the Regional Government of Andalusia. M.J. Polo wants to thank G. Gómez and J.A. Polo for
360 their valuable support.

361 **References**

362 Aguilar, C., Herrero, J., and Polo, M.J.: Topographic effects on solar radiation
363 distribution in mountainous watersheds and their influence on reference evapotranspiration
364 estimates at watershed scale, *Hydrol. Earth Syst. Sci.*, 14, 2479–2494, doi: 10.5194/hess-14-
365 2479-2010, 2010.

366 Alados, L., Jiménez, J.I., and Castro, Y.: Thermal radiation from cloudless skies in
367 Granada, *Theor. Appl. Climatol.*, 37, 84-89, 1986.

368 Armstrong, R.L., and Brun, E. (Eds.): *Snow and Climate. Physical Processes, Surface*
369 *Energy Exchange and Modeling*, Cambridge University Press, Cambridge, 2008.

370 Barbaro, E., Oliveira, A.P., Soares, J., Codato, G., Ferreira, M.J., Mlakar, P., Božnar,
371 M.Z., and Escobedo, J.F.: Observational Characterization of the Downward Atmospheric
372 Longwave Radiation at the Surface in the City of São Paulo, *J. Appl. Meteor. Climatol.*, 49,
373 2574–2590, doi: 10.1175/2010JAMC2304.1, 2010.

374 Brunt, D.: Notes on radiation in the atmosphere, *Q. J. R. Meteorol. Soc.*, 58. 389–418,
375 1932.

376 Brutsaert, W.: On a derivable formula for long-wave radiation from clear skies, *Water*
377 *Resour. Res.*, 11 ,742–744, 1975.

378 Brutsaert, W.: *Evaporation into the Atmosphere*, D. Reidel Publishing Company,
379 Dordrecht, 1982.

380 Crawford, T.M., and Duchon, C.E.: An improved parameterization for estimating
381 effective atmospheric emissivity for use in calculating daytime downwelling long-wave
382 radiation, *J. Appl. Meteorol.*, 38, 474–480, 1999.

383 Dera J.: *Marine physics*, Elsevier, Amsterdam, 1992.

384 Flerchinger, G.N., Xiao, W., Marks, D., Sauer, T.J., and Yu, Q.: Comparison of
385 algorithms for incoming atmospheric long-wave radiation, *Water Resour. Res.*, 45, W03423,
386 doi: 10.1029/2008WR007394, 2009.

387 Frigerio, E.: Radiación nocturna: campañas en Cachi, *Avances en Energías Renovables*
388 *y Medio Ambiente*, Vol. 8, nº 2, Argentina, 2004.

389 Gabathuler, M., Marty, C., and Hanselmann, K.W.: Parameterization of incoming
390 longwave radiation in high-mountain environments, *Phys. Geogr.*, 22, 99–114, 2001.

391 Herrero J., Polo, M.J., Moñino, A., and Losada, M.A.: An energy balance snowmelt
392 model in a Mediterranean site, *J. Hydrol.*, 371, 98-107, doi: 10.1016/j.jhydrol.2009.03.021,
393 2009.

394 Herrero, J., Aguilar, C., Millares, A., Moñino, A., Polo, M.J., and Losada, M.A.:
395 Mediterranean high mountain meteorology from continuous data obtained by a permanent

396 meteorological station at Sierra Nevada, Spain, EGU General Assembly, Vienna, Austria, 3-8
397 April 2011, EGU2011-12893, 2011.

398 Iziomon, M.G, Mayer, H., and Matzarakis, A.: Downward atmospheric irradiance under
399 clear and cloudy skies: measurement and parameterization, *J. Atm. Solar-Terr. Phys.*, *65*, 1107–
400 1116, doi:10.1016/j.jastp.2003.07.007, 2003.

401 Jordan, R. E., Andreas, E. L., and Makshtas, A. P.: Heat budget of snow-covered sea ice
402 at North Pole 4. *J. Geophys. Res.*, *104*(C4), 7785–7806, doi: 10.1029/1999JC900011, 1999.

403 Kimball, B.A., Idso, S.B., and Aase, J.K.: A model for thermal radiation from partly
404 cloudy and overcast skies, *Water Resour. Res.*, *18*, 931-936, 1982.

405 Kjaersgaard, J.H., Plauborg, F.L., and Hansen, S.: Comparison of models for
406 calculating daytime long-wave irradiance using long term data set, *Agric. Forest Meteorol.*,
407 *143*, 49-63, doi: 10.1016/j.agrformet.2006.11.007, 2007.

408 König-Langlo, G., and Augstein, E.: Parameterization of the downward long-wave
409 radiation at the Earth's surface in polar regions, *Meteorol., Z.* *3*, pp. 343–347, 1994.

410 Kustas, W.P., Rango, A., and Uijlenhoet, R.: A simple energy budget algorithm for the
411 snowmelt runoff model, *Water Resour. Res.*, *30*, 1515-1527, 1994.

412 Lhomme, JP, Vacher, JJ, and Rocheteau, A.: Estimating downward long-wave radiation
413 on the Andean Altiplano, *Agric. Forest Meteorol.*, *145*(3–4), 139–148, doi:
414 10.1016/j.agrformet.2007.04.007, 2007.

415 Marks, D., and Dozier, J.: A clear-sky longwave radiation model for remote alpine
416 areas, *Theor. Appl. Climatol.*, *27*, 159-187, doi: 10.1007/BF02243741, 1979.

417 Ohmura, A.: Physical Basis for the Temperature-Based Melt-Index Model, *J. Appl.*
418 *Meteorol.*, *40*, 753–761, 2001.

419 Philipona, R., Dürr, B., Marty, C., Ohmura, A., and Wild, M.: Radiative forcing -
420 measured at Earth's surface - corroborate the increasing greenhouse effect, *Geophys. Res. Lett.*,
421 *31*, L03202, doi: 10.1029/2003GL018765, 2004.

422 Pirazzini, R., Nardino, M., Orsini, A., Calzolari, F., Georgiadis, T., and Levizzani, V.:
423 Parameterization of the downward longwave radiation from clear and cloudy skies at Ny
424 Ålesund (Svalbard), in: *IRS 2000: Current Problems in Atmospheric Radiation*, 559–562, A.
425 Deepack Publishing, Hampton, Virginia, 2000.

426 Prata, A.P.: A new long-wave formula for estimating downward clear-sky radiation at
427 the surface, *Q. J. R. Meteorol. Soc.*, *122*, 1127–1151, doi: 10.1002/qj.49712253306, 1996.

428 Sedlar, J., and Hock, R.: Testing longwave radiation parameterizations under clear and
429 overcast skies at Storglaciären, Sweden, *The Cryosphere*, *3*, 75-84, doi: 10.5194/tc-3-75-2009,
430 2009.

431 Sicart, J. E., Pomeroy, J.W., Essery, R.L.H., and Bewley, D.: Incoming longwave
432 radiation to melting snow: observations, sensitivity and estimation in northern environments,
433 *Hydrol. Process.*, 20, 3697–3708, doi: 10.1002/hyp.6383, 2006.

434 Staiger, H., and Matzarakis, A.: Evaluation of atmospheric thermal radiation algorithms
435 for daylight hours, *Theor. Appl. Climatol.*, 102, 227–241, 2010.

436 Sugita, M., and Brutsaert, W.: Cloud Effect in the Estimation of Instantaneous
437 Downward Longwave Radiation, *Water Resour. Res.*, 29, 599–605, doi: 10.1029/92WR02352,
438 1993.

439 Unsworth, M. H., and Monteith, J.L.: Long-wave radiation at the ground. I. Angular
440 distribution of incoming radiation, *Q. J. R. Meteorol. Soc.*, 101, 13-24, doi:
441 10.1002/qj.49710142703, 1975.

442 Weiss, A.: On the performance of pyrgeometers with silicon domes, *J. Appl. Meteorol.*,
443 20, 962-965, 1981.

444

445

446 **Table 1.** Summary of the goodness of agreement for the new 3-state parameterization (3-
 447 sParam, Eqs. (4) to (7)), the modified Brutsaert's equation (modB82, Eqs. (7) and (8)), the
 448 same modB82 with a variable leading coefficient (modB82, with Eq (9)) and Crawford and
 449 Duchon (1999) (CD99) for different atmospheric states for the calibration and validation
 450 datasets. MAE: Mean Absolute Error; RMSE: Root Mean Square Error.

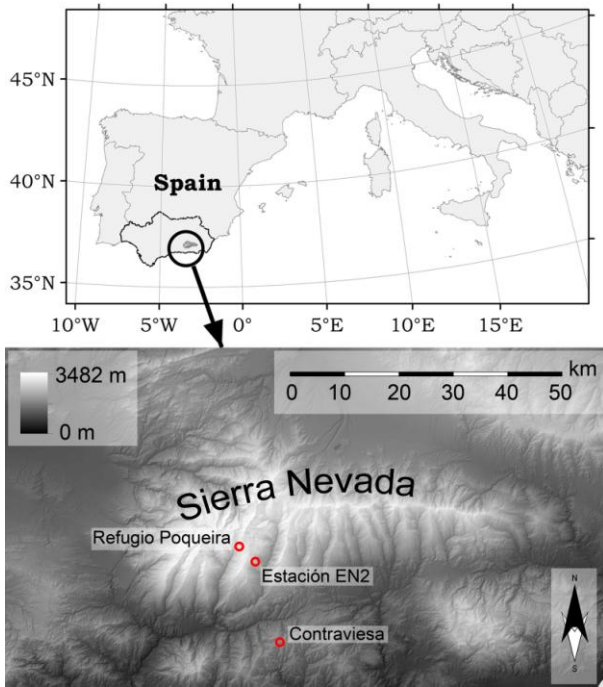
451

Atmospheric state	3-sParam	modB82	modB82-var	CD99
	MAE/RMSE	MAE/RMSE	MAE/RMSE	MAE/RMSE
Calibration. RP Station (Nov2004-Dec2010)				
Daytime. All data	0.045/0.066	0.060/0.078	0.056/0.076	0.058/0.080
- Clear skies	0.037/0.055	0.058/0.073	0.049/0.069	0.049/0.069
- Covered skies	0.025/0.040	0.042/0.057	0.042/0.056	0.069/0.084
- Partly cloudy	0.070/0.092	0.075/0.096	0.077/0.096	0.075/0.098
Validation. RP Station (Jan2011-Dec2011)				
Daytime. All data	0.049/0.068	0.070/0.087	0.064/0.084	0.065/0.086
- Clear skies	0.045/0.062	0.073/0.088	0.061/0.082	0.060/0.081
- Covered skies	0.031/0.048	0.048/0.062	0.056/0.067	0.078/0.095
- Partly cloudy	0.067/0.087	0.075/0.094	0.077/0.095	0.071/0.094
Validation. C Station (Aug2004-Apr2012)				
Daytime. All data	0.071/0.084	0.041/0.054	0.052/0.065	0.053/0.067
- Clear skies	0.084/0.092	0.041/0.050	0.059/0.068	0.057/0.068
- Covered skies	0.027/0.038	0.026/0.40	0.024/0.039	0.049/0.064
- Partly cloudy	0.072/0.087	0.047/0.062	0.054/0.069	0.049/0.066
Validation. EN2 Station (Oct2009-Mar2012)				
Daytime. All data	0.043/0.055	0.060/0.077	0.075/0.088	0.074/0.088
- Clear skies	0.041/0.053	0.049/0.060	0.067/0.076	0.068/0.077
- Covered skies	0.024/0.033	0.049/0.063	0.058/0.068	0.070/0.081
- Partly cloudy	0.057/0.069	0.092/0.111	0.103/0.119	0.090/0.113

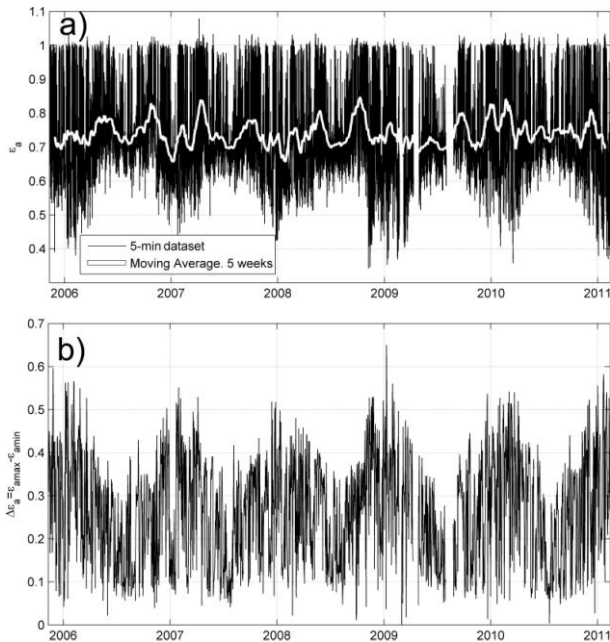
452

453

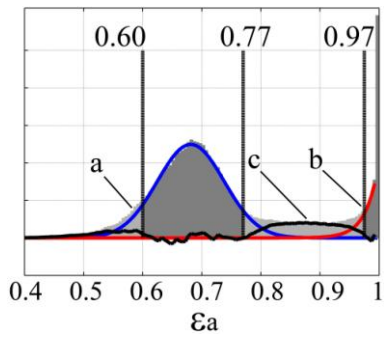
454 **Fig. 1.** Location of Sierra Nevada in Andalusia, Spain, and weather stations on Southern slope
455 used.



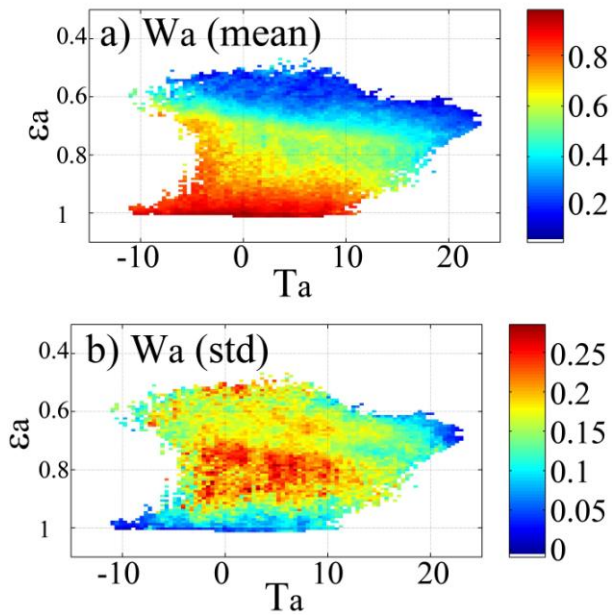
456
457 **Fig. 2.** Atmospheric emissivity measured at RP station from 2005 to 2011. (a) Complete
458 dataset with 5-min frequency and the 5-weeks moving average in white. (b) Daily variation
459 (difference between maximum and minimum daily values).



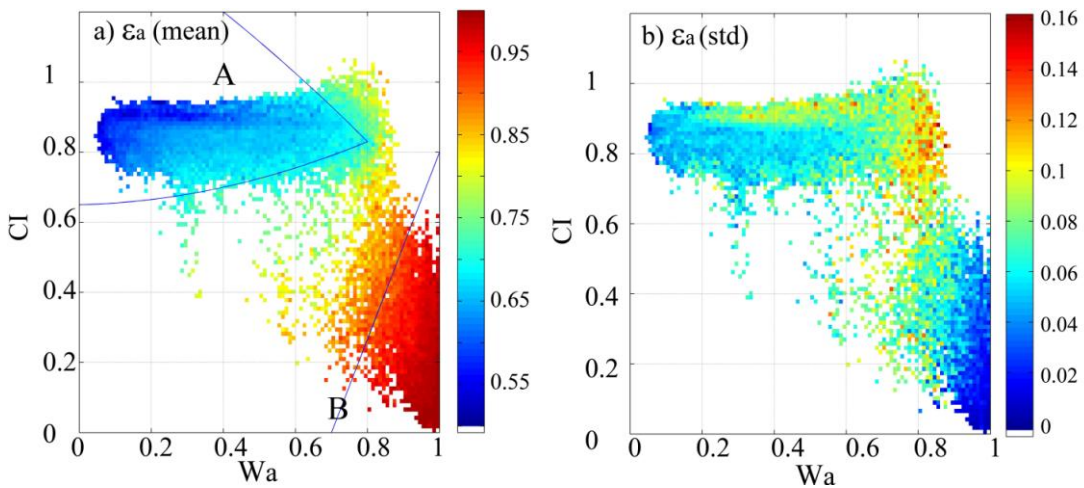
460
461 **Fig. 3.** Pdf of the atmospheric emissivity 5-min values from 2005 to 2011 with a Gaussian fit
462 for clear sky conditions, b exponential fit for completely covered data and c residual
463 corresponding to partly covered sky situations.



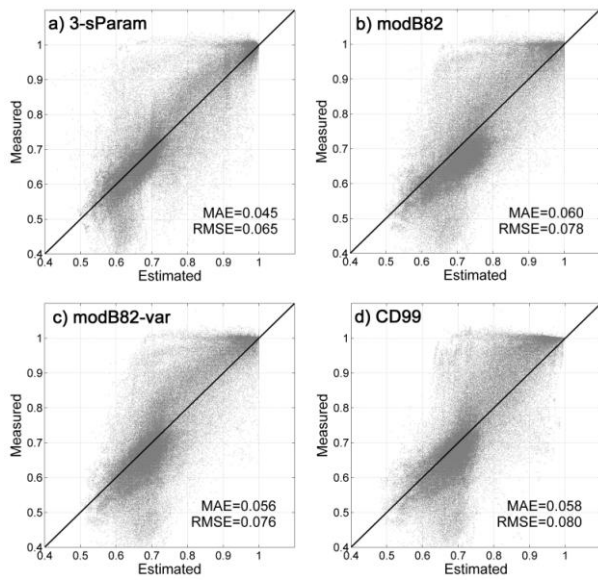
464
 465 **Fig. 4.** (a) Mean value and (b) standard deviation for relative humidity W_a measurements as a
 466 function of temperature T_a and atmospheric emissivity ϵ_a .



467
 468 **Fig. 5.** (a) Mean value and (b) standard deviation for atmospheric emissivity measurements as
 469 a function of CI and W_a .



470
 471 **Fig. 6.** Atmospheric emissivity measurements versus estimation obtained for the calibration at
 472 RP Station (2500 m a.s.l.) using the four different models.

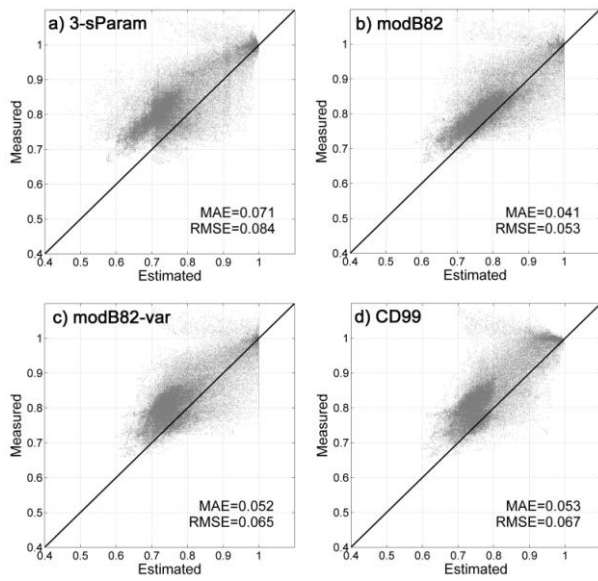


473

474

475

Fig. 7. Atmospheric emissivity measurements versus estimation obtained for the validation at C Station (1332 m a.s.l.) using the four different models.



476